



# Cyclophilin D deficiency attenuates mitochondrial F1Fo ATP synthase dysfunction via OSCP in Alzheimer's disease

Esha Gauba, Hao Chen, Lan Guo, Heng Du\*

Department of Biological Sciences, The University of Texas at Dallas, United States

## ARTICLE INFO

### Keywords:

Alzheimer's disease  
Mitochondrial F1Fo ATP synthase  
Oligomycin sensitivity conferring protein  
Cyclophilin D  
A $\beta$

## ABSTRACT

Mitochondrial dysfunction is pivotal in inducing synaptic injury and neuronal stress in Alzheimer's disease (AD). Mitochondrial F1Fo ATP synthase deregulation is a hallmark mitochondrial defect leading to oxidative phosphorylation (OXPHOS) failure in this neurological disorder. Oligomycin sensitivity conferring protein (OSCP) is a crucial F1Fo ATP synthase subunit. Decreased OSCP levels and OSCP interaction with amyloid  $\beta$  (A $\beta$ ) constitute key aspects of F1Fo ATP synthase pathology in AD-related conditions. However, the detailed mechanisms promoting such AD-related OSCP changes have not been fully resolved. Here, we have found increased physical interaction of OSCP with Cyclophilin D (CypD) in AD cases as well as in an AD animal model (5xFAD mice). Genetic depletion of CypD mitigates OSCP loss via ubiquitin-dependent OSCP degradation in 5xFAD mice. Moreover, the ablation of CypD also attenuates OSCP/A $\beta$  interaction in AD mice. The relieved OSCP changes by CypD depletion in 5xFAD mice are along with preserved F1Fo ATP synthase function, restored mitochondrial bioenergetics as well as improved mouse cognition. The simplest interpretation of our results is that CypD is a critical mediator that promotes OSCP deficits in AD-related conditions. Therefore, to block the deleterious impact of CypD on OSCP has the potential to be a promising therapeutic strategy to correct mitochondrial dysfunction for AD therapy.

## 1. Introduction

Alzheimer's disease (AD) is a devastating neurodegenerative disorder characterized by progressive cognitive decline (Cummings, 2004). Previous studies have repeatedly identified that mitochondrial dysfunction is a hallmark brain pathology underlying AD synaptic injury and neuronal death (Reddy et al., 2010; Wang et al., 2014; Zhu et al., 2013). Compromised mitochondrial oxidative phosphorylation (OXPHOS) constitutes a characteristic mitochondrial deficit in AD brains, resulting in lowered ATP production and increased oxidative stress, and eventually cell death (Du et al., 2012; Reddy, 2006; Reddy and Beal, 2008). The detailed mechanisms of OXPHOS impairment in AD remain as a long-standing scientific issue. But emerging evidence has accentuated the role of mitochondrial F1Fo ATP synthase dysfunction in AD-related mitochondrial OXPHOS failure (Beck et al., 2016).

Mitochondrial F1Fo ATP synthase is the executive site for ADP phosphorylation (He et al., 2018; Rubinstein et al., 2003). The dysfunction of this critical mitochondrial enzyme leads to disrupted OXPHOS and progressive ATP depletion. It is suggested that the AD-related F1Fo ATP synthase deregulation is strongly associated with the

aberrations of its key subunit, oligomycin sensitivity conferring protein (OSCP) (Beck et al., 2016). OSCP is part of the peripheral stalk of F1Fo ATP synthase and plays a vital role in maintaining the structural stability of F1Fo complex (Carbajo et al., 2007). Decreased expression of OSCP and the physical interaction of OSCP with amyloid  $\beta$  (A $\beta$ ) cause the loss of OSCP function, culminating in the deregulation of F1Fo ATP synthase in AD-related conditions (Beck et al., 2016). In this regard, to determine the causative factors for such OSCP dysfunction is of paramount importance to understand mitochondrial OXPHOS defects in AD.

Intriguingly, a previous study on aging mice has shown an unexpected regulation on OSCP expression by Cyclophilin D (CypD; gene name: *Ppif*), which is evidenced by the observation that the brain aging-related OSCP loss is rescued by genetic depletion of CypD (Gauba et al., 2017). Given the close relationship of brain aging and AD, it is possible that decreased OSCP expression levels in AD brains are as well a result of CypD effect as increased CypD expression levels are a determined AD brain pathology (Du et al., 2008; Du et al., 2011). Furthermore, CypD has the capacity to bind both OSCP (Beutner et al., 2017; Giorgio et al., 2009) and A $\beta$  (Du et al., 2008; Du et al., 2011). Of note, the interaction of CypD with OSCP could potentiate F1Fo complex uncoupling (Gauba et al., 2017; Giorgio et al., 2009); while the interplay of CypD with A $\beta$

\* Corresponding author at: Department of Biological Sciences, The University of Texas at Dallas, 800 W. Campbell Rd., Richardson, TX 75080, United States.  
E-mail address: [heng.du@utdallas.edu](mailto:heng.du@utdallas.edu) (H. Du).

enhances CypD function (Du et al., 2008). Therefore, A $\beta$  might serve as a key mediator that intensifies the deleterious effect of CypD on OSCP in AD-related conditions. On the other side, CypD may potentially affect the interaction of OSCP with A $\beta$ . In this context, we thus hypothesize that CypD may play a crucial role in promoting OSCP changes in AD brains.

To this end, we examine the effect of CypD on OSCP in an AD animal model that mimics AD-like brain amyloidosis (5xFAD mice). We aim to determine whether CypD is a regulatory factor for OSCP expression and function in A $\beta$ -rich milieu. In addition, we also examine whether ablation of CypD could be a practical strategy to protect OSCP in AD-related conditions.

## 2. Results

### 2.1. A $\beta$ enhances CypD and OSCP interaction in AD subjects and 5xFAD mice

To determine the status of CypD and OSCP interplay in AD-related conditions, we subjected temporal lobe extracts from AD and nonAD subjects to perform co-immunoprecipitation for CypD and OSCP interaction. AD cases demonstrated significantly increased CypD/OSCP complexes (Fig. 1a1&2, Supplementary Table 1), suggesting enhanced CypD and OSCP interaction in AD brains. Next, we examined CypD/OSCP complexes in 5xFAD mice by antibody-based Duolink<sup>®</sup> proximity ligation assay (PLA). PLA is a sensitive method to visualize and quantify tissue-based direct protein interactions in situ (Koos et al., 2014; Lutz et al., 2017). 5xFAD mice exhibited substantially increased density of CypD/OSCP complexes in their neocortex in an age-dependent manner (Fig. 1b1&2). These results seem to implicate enhanced regulatory effect of CypD on OSCP in AD-related conditions.

Of note, by immunofluorescent staining as well as immunoblotting we have seen an age-dependent increase in CypD expression levels (Fig. 1c1&2, d1&2) along with decreased OSCP expression (Fig. 1c1&3, d1&3) in 5xFAD mice, which are consistent with our previous observations with AD subjects and AD mouse models (Beck et al., 2016; Du et al., 2008, 2010). Given lowered expression levels of OSCP should disfavor the formation of CypD/OSCP complexes, we then asked whether A $\beta$  promotes OSCP/CypD interaction. To this end, we employed in vitro pull-down assays using glutathione S-transferase (GST)-tagged OSCP as the bait protein. As shown in Fig. 1e1–4, when A $\beta$  was added, the equilibrium dissociation constant ( $K_D$ ) of CypD/OSCP interaction was substantially decreased from  $0.1 \pm 0.015 \mu\text{M}$  (w/o A $\beta$ ) to  $0.06 \pm 0.001 \mu\text{M}$  (with A $\beta$ ), indicating a tighter binding of CypD with OSCP in the presence of A $\beta$ .

### 2.2. CypD deficiency attenuates mitochondrial F1Fo ATP synthase deregulation in 5xFAD mice

Previous studies indicate the deleterious influence of CypD and OSCP interaction on F1Fo ATP synthase function (Gauba et al., 2017; Giorgio et al., 2009). If increased CypD/OSCP complex formation as seen in 5xFAD mice underlies F1Fo ATP synthase dysfunction, we would expect a protective effect of CypD deficiency. To this end, we established CypD-knockout 5xFAD (*Ppif*<sup>-/-</sup>/5xFAD) mice. Of note, CypD had little impact on the levels of brain A $\beta$  deposition in mice at both tested ages (4 and 9 months old) (Fig. 2a1&2), which is in consistency with our previous observations (Du et al., 2008). The similar levels of soluble A $\beta$ 1–40 (Fig. 2a3) and A $\beta$ 1–42 (Fig. 2a4) in 5xFAD mice with or without CypD expression were further determined by A $\beta$  ELISA assay. To reflect F1Fo ATP synthase function, we examined F1Fo ATP synthase catalytic activity in neuron-specific synaptic mitochondria. In sharp contrast to their 5xFAD littermates, CypD-deficient 5xFAD mice exhibited substantially preserved F1Fo ATP synthase enzymatic activity at both 4 and 9 months old of age (Fig. 2b1&2). Further examination of F1Fo ATP synthase coupling assay showed a significant

protection by CypD depletion (Fig. 2c1&2), indicating preserved F1Fo complex proton-flow coupling against A $\beta$  toxicity. As a result of protected F1Fo ATP synthase function by CypD deficiency, we have observed remarkably improved synaptic mitochondrial respiratory control ratio (RCR) (Fig. 2d1&2) as well as restored ATP production (Fig. 2e1&2) in CypD deficient 5xFAD mice at both 4 and 9 months old. The above results suggest that CypD modulates F1Fo ATP synthase dysfunction in AD-related conditions.

### 2.3. CypD promotes OSCP loss via ubiquitination in 5xFAD mice

To determine whether the effect of CypD on neuronal mitochondrial F1Fo ATP synthase is associated with OSCP, we examined the influence of CypD on OSCP expression in 5xFAD mice. Purified synaptic mitochondria from nonTg, CypD deficient, 5xFAD and CypD deficient 5xFAD mice at 4 and 9 months old were subjected to immunoblotting assays for OSCP expression. In parallel, the expression levels of other major F1Fo ATP synthase subunits including  $\alpha$ ,  $\beta$ ,  $\gamma$ , and a, b, c were also measured. There was little or no genotypic phenotype of CypD deficiency on the expression levels of other major subunits regardless of the presence or absence of A $\beta$  (Fig. 3a1&2). However, CypD deficient 5xFAD mice exhibited remarkably preserved OSCP levels at both tested ages in comparison with their age- and gender-matched 5xFAD littermates (Fig. 3b1&2), implicating the effect of CypD on OSCP levels. This was further confirmed by our experiments using CypD-overexpressing neurons that showed selective decrease in OSCP expression levels (Fig. 3c). Since the proteolysis via the ubiquitin system is a critical pathway for OSCP degradation (Margineantu et al., 2007), we then examined whether CypD potentiates OSCP ubiquitination in 5xFAD mice. As expected, increased OSCP ubiquitination was detected in 5xFAD brains in both 4 and 9 months old mice, which was significantly attenuated by CypD depletion (Fig. 3d1&2). Put together, the results suggest that CypD is a mediator of OSCP loss in 5xFAD mice probably by promoting OSCP degradation via ubiquitination.

### 2.4. CypD promotes OSCP/A $\beta$ interaction in 5xFAD mice

CypD, OSCP and A $\beta$  bind to each other (Beck et al., 2016; Du et al., 2008; Gauba et al., 2017). Since A $\beta$  could alter the binding affinity of CypD with OSCP (Fig. 1e1–4), it is thus of great interest to determine whether CypD has the similar effect on OSCP and A $\beta$  interaction. In this regard, we adopted GST-tagged OSCP as the bait protein and performed in vitro pull down assays to examine the binding affinity of OSCP with A $\beta$  in the absence or presence of CypD. Intriguingly, we found that the  $K_D$  of OSCP/A $\beta$  interaction was dramatically decreased from  $0.51 \pm 0.071 \mu\text{M}$  (w/o CypD) to  $0.088 \pm 0.043 \mu\text{M}$  (with CypD) (Fig. 4a1–4), indicating that CypD augments OSCP and A $\beta$  interaction. If this in vitro observation could be extrapolated into an in vivo setting, we would expect to see less OSCP/A $\beta$  complexes in CypD deficient 5xFAD mice. Indeed, our PLA results showed a significant decrease of OSCP/A $\beta$  complex density in the neocortex of *Ppif*<sup>-/-</sup>/5xFAD mice in comparison with their age- and gender-matched 5xFAD littermates at 4 and 9 months old (Fig. 4b1&2), despite the age-dependent increase of OSCP/A $\beta$  interaction in all the tested A $\beta$ -producing mice (Fig. 4b1&2). Therefore, together with the observations on OSCP expression our findings indicate that CypD is a critical promoting entity underlying OSCP pathology in AD-relative pathological settings.

### 2.5. CypD deficiency improves cognitive function in 5xFAD mice

The close correlation of mitochondrial dysfunction with cognitive deficits has been repeatedly identified in AD patients as well as AD animal models. Consistent with alleviated F1Fo ATP synthase function, CypD deficient 5xFAD mice at both tested ages exhibited rescued spatial reference learning and memory (Fig. 5a1&2, b1&2) with unaltered swimming speed (Fig. 5c1&2) when comparing with their age- and

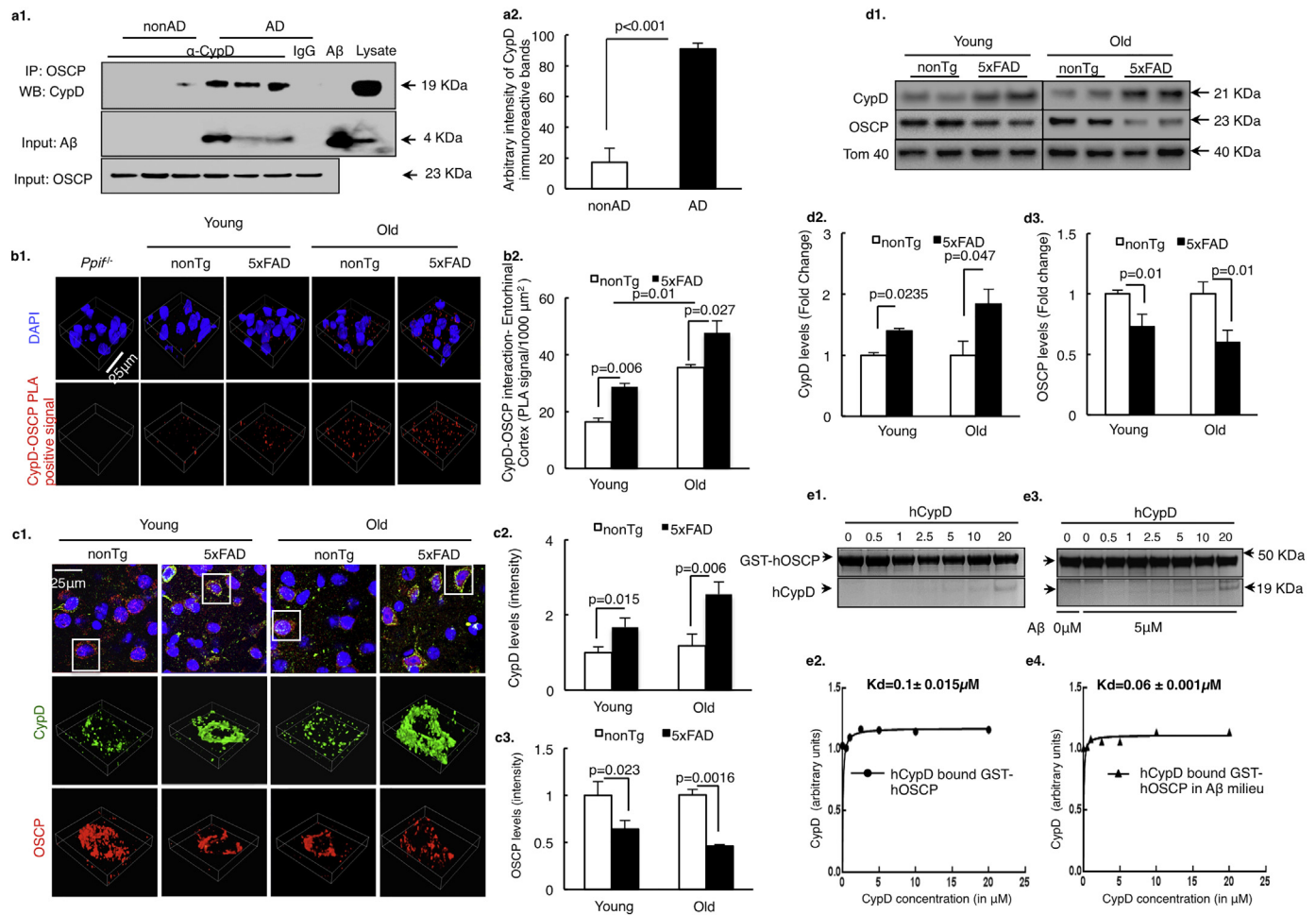


**Fig. 1.** A $\beta$  enhances CypD and OSCP interaction.

(a) Co-immunoprecipitation of CypD and OSCP in AD patient temporal lobe extracts. Results shown are representative from three non-AD and three AD patients. AD brain lysate were used as positive controls for CypD and A $\beta$  immunoreactive bands. A $\beta$  peptide was used as positive control for A $\beta$  immunoreactive bands. (b) OSCP and CypD interaction determined by in situ PLA assay in 5xFAD mouse neocortex. Scale bar, 25  $\mu$ m.  $n = 6$  for nonTg and 5xFAD groups in both young and old mice. *Ppif*<sup>-/-</sup> mice were used as a negative control. (c) Monitoring the changes in OSCP and CypD expression levels in young and old nonTg and 5xFAD mouse brain showed inverse changes. Scale bar, 25  $\mu$ m.  $n = 5$  per group. Quantification of staining intensity for CypD and OSCP in young and old nonTg and 5xFAD mouse brain showed inverse changes. (d) Representative immunoreactive bands for expression levels of CypD and OSCP in young and old nonTg and 5xFAD mouse synaptic mitochondria. CypD expression levels were upregulated while OSCP expression levels were downregulated in synaptic mitochondria from 5xFAD mice in an age-dependent manner.  $n = 5$ –6 per group. (e) OSCP and CypD interaction determined by an in vitro pull-down assay. The assay showed that A $\beta$  enhances the ability of CypD to bind to OSCP. Error bars represent s.e.m.

gender-matched 5xFAD littermates. The results are in agreement with our previous findings on another AD mouse model (J20 line) (Du et al., 2008), further suggesting that the protection on cognition by CypD deficiency is not AD mouse model-sensitive but rather related to its protection on mitochondrial function.

### 3. Discussion

As the major source of energy via oxidative phosphorylation (OXPHOS), mitochondria are essential organelles for neuronal physiology and survival. In recent years, mitochondrial cascade hypothesis has become a central paradigm in studying Alzheimer's disease (AD), in particular its sporadic form (Swerdlow et al., 2014). Compromised mitochondrial OXPHOS is a determined brain pathology that induces synaptic and neuronal stress in this neurological disorder (Du et al., 2010; Manczak et al., 2004; Mastroeni et al., 2017; Onyango et al., 2016; Wang et al., 2016; Yao et al., 2009). As a result, the detailed molecular mechanisms of defected mitochondrial bioenergetics in AD have become a critical scientific question. Recent recognition of mitochondrial F1Fo ATP synthase deregulation in AD cases and AD animal

models has substantially fostered our understanding of the pathogenesis of mitochondrial OXPHOS failure in AD (Beck et al., 2016). Importantly, the contribution of OSCP changes to this AD-related F1Fo ATP synthase dysfunction can be a potential target for AD therapy. Here, we have found that CypD plays a crucial role in mediating OSCP loss and OSCP/A $\beta$  interaction in AD-related conditions. The ablation of CypD alleviates these AD-associated OSCP aberrations and further mitigates F1Fo ATP synthase deregulation as well as mitochondrial bioenergetics deficits and cognitive decline in 5xFAD mice. These findings have suggested a novel therapeutic strategy to protect OSCP and F1Fo ATP synthase in AD. Moreover, the current research has revealed a key role of CypD in regulating mitochondrial bioenergetics, particularly in diseases.

CypD is a mitochondrial peptidyl prolyl cis/trans isomerase (PPIase) (Baines et al., 2005). PPIases are ubiquitous enzymes that affect the structural folding of their substrate proteins by catalyzing the *cis/trans* isomerisation of peptides immediately preceding proline residues (Wedemeyer et al., 2002; Wu and Matthews, 2002). As a member of PPIase family in mitochondria, CypD is proposed to mediate the folding and rearrangement of mitochondrial proteins such as the adenine

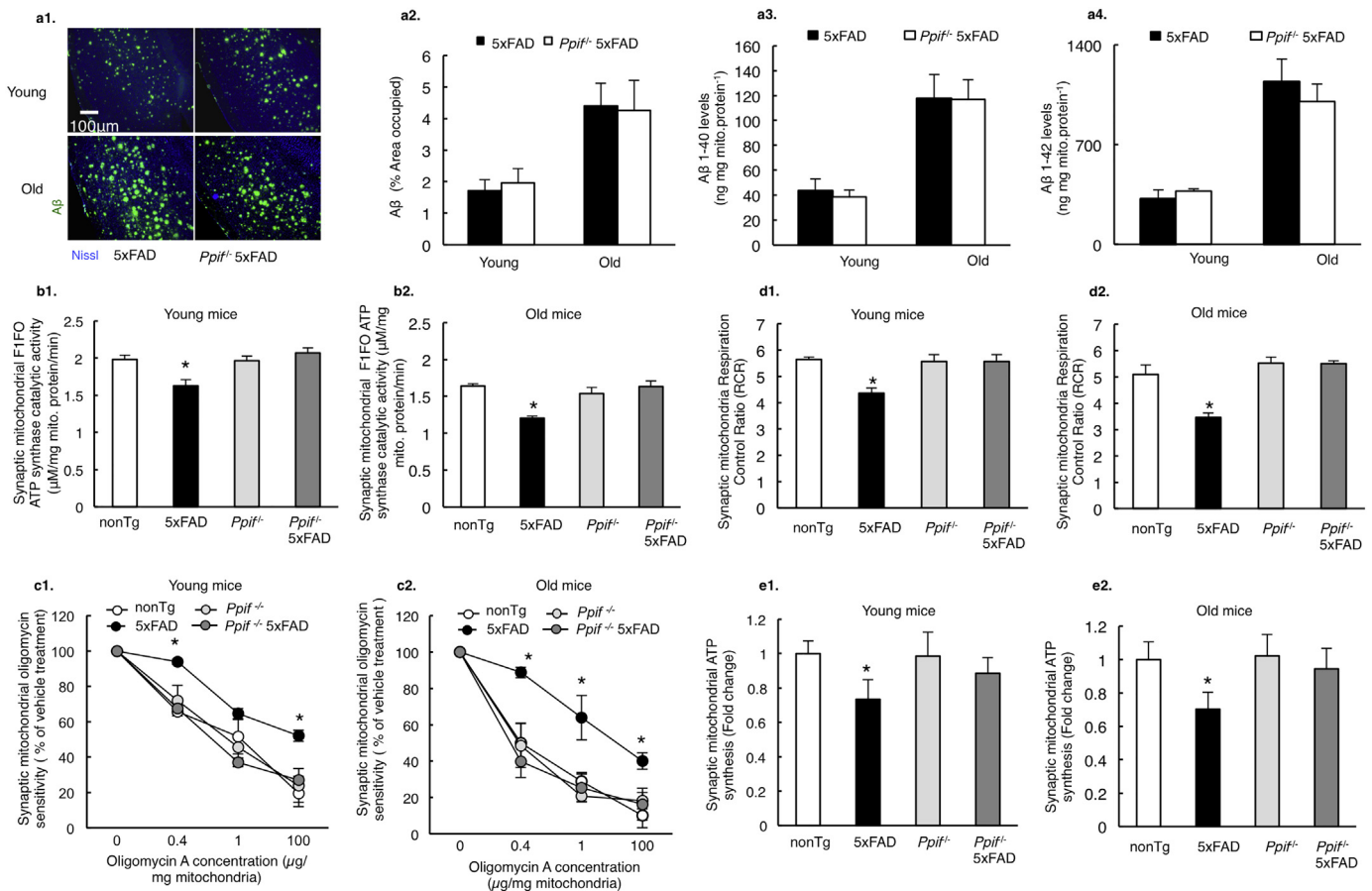


**Fig. 2.** CypD deficiency attenuates mitochondrial F1Fo ATP synthase deregulation in 5xFAD mice.

(a) Aβ levels in 5xFAD and CypD deficient 5xFAD mice at young and old age.  $n = 6$  for each group. Scale bar, 100 μm. ELISA on isolated synaptic mitochondria showed similar levels of Aβ 1–40 and Aβ 1–42 in both AD genotype mice. (b) Synaptic mitochondria from 5xFAD mice demonstrated blunted F1Fo ATP synthase catalytic activity, which exacerbates with age. This defect was protected by CypD deficiency in both young and old *Ppif*<sup>-/-</sup> 5xFAD mice.  $n = 5–7$  per group.  $*P < .05$  vs other groups. (c) Decreased oligomycin sensitivity of synaptic mitochondria from young and old 5xFAD mice were rescued by CypD deficiency. All data are presented as percentage of the activity of the corresponding vehicle-treated mitochondrial fractions.  $n = 5–7$  per group.  $*P < .05$  vs other groups. (d) Synaptic mitochondria from 5xFAD mice showed an age-dependent decrease in RCR, which was protected by CypD depletion.  $n = 5–7$  mice per group.  $*P < .05$  vs other groups (e) Synaptic mitochondria from 5xFAD mice demonstrated an age dependent decline in ATP synthesis as compared to other groups. This defect was protected in CypD deficient mice brain mitochondria.  $n = 5–7$  mice per group.  $*P < .05$  vs other groups. Error bars represent s.e.m.

nucleotide translocase (ANT), mitochondrial P53 and many others (Dahout-Gonzalez et al., 2006; Lebedev et al., 2016; Woodfield et al., 1998). In recent years, the impact of CypD on mitochondrial F1Fo ATP synthase has been highlighted to be a critical mechanism regulating mitochondrial bioenergetics in health and disease (Beutner et al., 2017; Chinopoulos et al., 2011; Gauba et al., 2017; Giorgio et al., 2009, 2010). OSCP is one of the determined CypD interacting proteins in F1Fo ATP synthase (Gauba et al., 2017; Giorgio et al., 2009). The interaction of CypD with OSCP is suggested to induce uncoupling of F1Fo ATP synthase, thus reducing the activity of this pivotal mitochondrial enzyme (Gauba et al., 2017; Giorgio et al., 2009). This process might play a critical role in modulating mitochondrial bioenergetics at physiological states (Beutner et al., 2017; Giorgio et al., 2009). But in pathological settings such as brain aging (Gauba et al., 2017) as well as AD as showed here, increased CypD interaction with OSCP is strongly associated with F1Fo ATP synthase deregulation, suggesting its relevance to diseases. Therefore, the dual roles of CypD regulation on OSCP in physiology and pathology seem to raise a dilemma, which forms a groundwork for our future investigation to establish a delicate strategy to block excess CypD impact on OSCP while preserving its physiological function.

Of note, although it is not yet clear how CypD interaction with OSCP alters OSCP function, a possible reason is that CypD mediates the

rearrangement of OSCP through their physical contact. Changes in the structural folding of a protein not only influence its function, but also potentially affect its capacity to form complexes with other entities such as proteins, peptides, and/or ions. This explains our observation that the interaction of CypD with OSCP causes an increment in OSCP/Aβ interaction. Indeed, we cannot fully exclude the possibility that increased OSCP/Aβ interaction is at least in part a result of the formation of CypD/OSCP/Aβ complexes. Moreover, it should be noted that we have also detected a promoting effect of Aβ on OSCP/CypD interaction. This might be due to increased CypD activity by Aβ, and/or the influence of Aβ on OSCP structure which makes its binding with CypD easier. Further study into these issues will help to address the above questions. Nevertheless, the current results suggest that blockade of CypD has the potential to relieve the deleterious impact of Aβ on OSCP through attenuated Aβ/OSCP interaction.

Another critical finding of this study that merits discussion is the role of CypD in modulating OSCP expression levels. We have found an inverse relationship between CypD and OSCP in 5xFAD mice. It should be noted that we have also seen significantly lowered OSCP levels in CypD overexpressing neurons. Importantly, our unpublished data shows that upregulation of OSCP in neurons *in vivo* had little influence on CypD levels. Therefore, the expression levels or the functional status of CypD seems to play a dominant role in regulating OSCP levels.

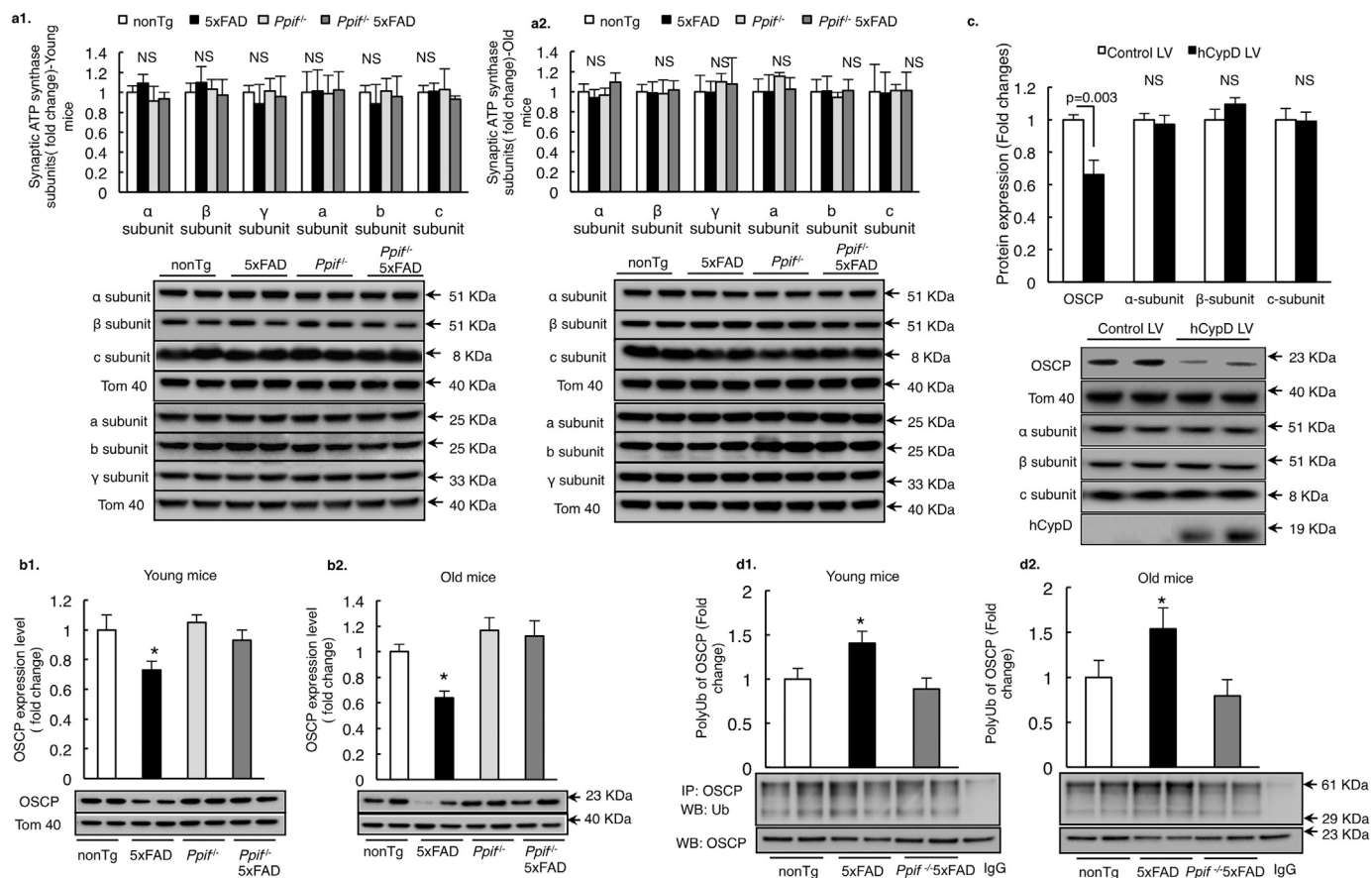


**Fig. 3.** CypD promotes OSCP loss via ubiquitination in 5xFAD mice.

(a) Densitometric quantification of the immunoreactive bands of major F1Fo ATP synthase subunits including  $\alpha$ ,  $\beta$ , c, a, b,  $\gamma$  subunits in synaptic mitochondria of young and old nonTg,  $Ppif^{-/-}$  mice and their AD counterparts.  $n = 6-10$  mice per group. The lower panels are representative immunoreactive bands. Tom40 was used as the loading control. (b) Densitometric quantification of the immunoreactive bands of OSCP in synaptic mitochondria of young and old nonTg,  $Ppif^{-/-}$  mice and their A $\beta$ -expressing counterparts.  $n = 6-10$  mice per group. The lower panels are representative immunoreactive bands. Tom40 was used as the loading control. \* $P < .05$  vs other groups. (c) OSCP expression was downregulated in primary cultured mouse neurons by hCypD overexpression. Other major F1Fo ATP synthase subunits like  $\alpha$ ,  $\beta$  and c subunit displayed no change in expression levels. The lower panels are representative immunoreactive bands of indicated proteins. Tom 40 was used as the loading control.  $n = 3$  independent experiments. (d) Mouse brain mitochondria from nonTg, 5xFAD and  $Ppif^{-/-}$  5xFAD mice were subjected to immunoprecipitation with OSCP antibody followed by immunoblotting with ubiquitin and OSCP. Results are representative from 6 mice per group for both young and old age. \* $P < .05$  vs other groups. Error bars represent s.e.m.

Although the detailed mechanisms of CypD-mediated OSCP downregulation are not yet resolved, our results have suggested OSCP degradation via ubiquitination. According to the prevailing opinions, the ubiquitin-dependent proteolysis is not generally accepted to be a pathway for mitochondrial protein degradation. However, increasing evidence has revealed a role of ubiquitin-mediated degradation of some mitochondrial proteins including OSCP (Heo and Rutter, 2011; Lehmann et al., 2016; Margineantu et al., 2007). It is suggested that OSCP undergoes retrograde transport to outer mitochondrial membrane (OMM), where OSCP is subsequently degraded via ubiquitination (Margineantu et al., 2007). Indeed, we have found increased ubiquitinated OSCP in 5xFAD mice, suggesting that enhanced OSCP ubiquitination is closely associated with OSCP loss in AD-related conditions. Moreover, the remarkable inhibition of OSCP ubiquitination by CypD deficiency also adds credit to the hypothesis that there is a potential link between CypD and OSCP degradation. A possible mechanism is that CypD alters the structure of OSCP and/or promotes OSCP/A $\beta$  interaction, which mediates accelerated OSCP turnover. Since our understanding of CypD in ubiquitin-dependent proteolysis pathway is extremely limited, the detailed mechanisms of CypD-related OSCP degradation needs further study.

In summary, we have established a model in which CypD plays a key role in OSCP aberrations in AD-related pathological settings,

leading to F1Fo ATP synthase dysfunction and the resultant mitochondrial defects, eventually causing neuronal injury and death (Fig. 6). The ablation of CypD has demonstrated significant protection on mitochondrial F1Fo ATP synthase function as well as mitochondrial bioenergetics. Indeed, we cannot exclude that the protective effects of CypD deficiency are also associated with other mechanisms such as the modulation of mitochondrial protein acetylation (Nguyen et al., 2013), the inhibition of mitochondrial permeability transition (Baines et al., 2005; Du and Yan, 2010), and the attenuation of changes of other mitochondrial proteins. Nevertheless, the results have at least suggested that CypD-mediated OSCP dysfunction is a pivotal mechanism of mitochondrial F1Fo ATP synthase deregulation and the resultant OXPHOS failure in AD-related pathological settings. Therefore, the most parsimonious interpretation of the results is that the interplay between CypD and OSCP in A $\beta$ -rich milieu is a primary AD change that potentially causes mitochondrial defects.

## 4. Methods

### 4.1. Mice

Animal studies were performed under the guidelines of International Animal Care and Use Committee (IACUC) at University of

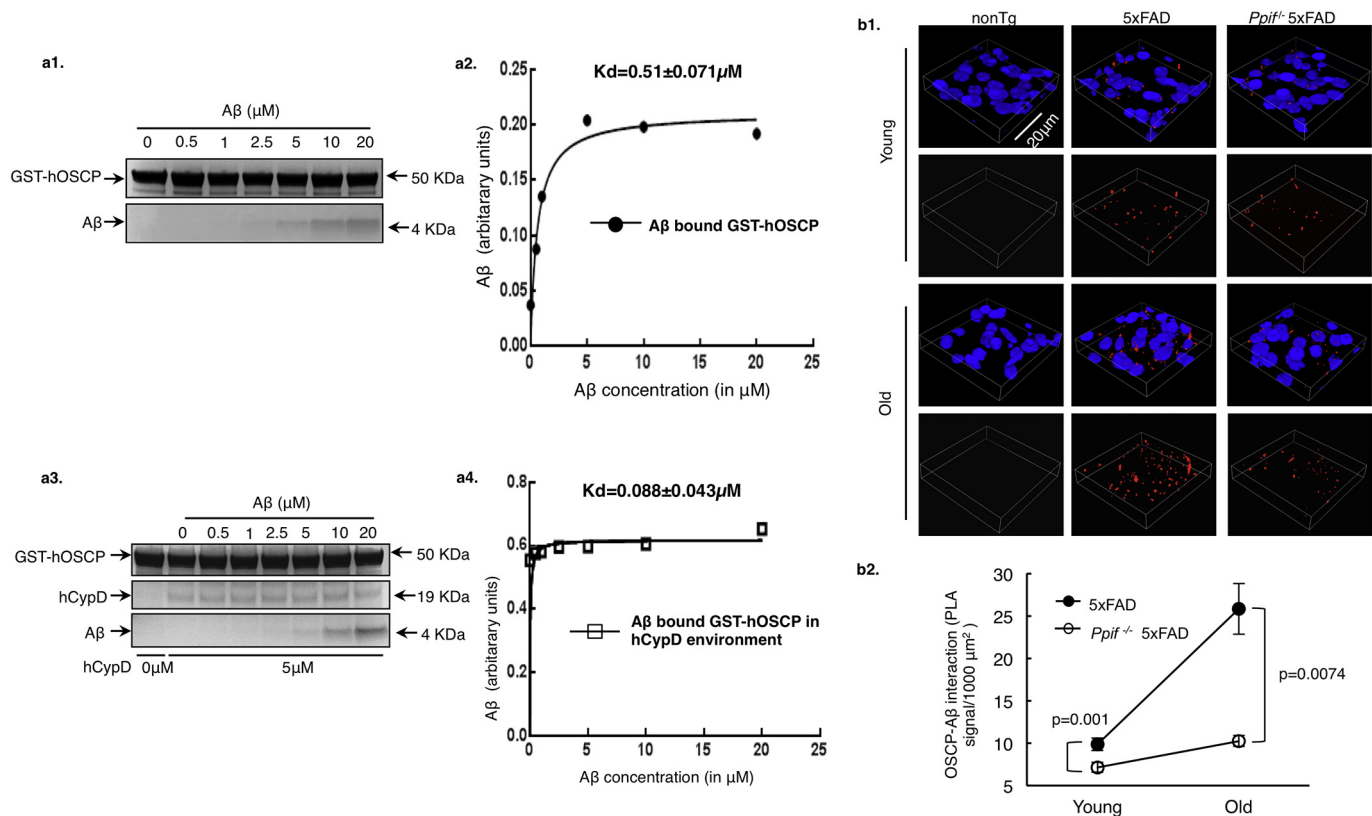


**Fig. 4.** CypD promotes OSCP/Aβ interaction in 5xFAD mice.

(a) In vitro pull-down assay showed higher binding affinity of OSCP with Aβ in CypD rich environment. (b) In situ determination of OSCP and Aβ binding using proximity ligation assay in 5xFAD and *Ppif*<sup>-/-</sup> 5xFAD mice at young and old age. nonTg mouse brain was used as a negative control.  $n = 5-6$  for 5xFAD and *Ppif*<sup>-/-</sup> 5xFAD groups at both ages. Scale bar, 20 μm. Error bars represent s.e.m.

Texas at Dallas and National Institute of Health. Cyclophilin D deficient mice (B6;129-*Ppif*<sup>tm1Maf/J</sup>) and AD mice (B6SJL-Tg (APP<sup>SWFlon</sup>,PSEN1\*<sup>M146L</sup>\*L286V)6799Vas/Mmjax) were purchased from Jackson Laboratory. We crossed these two transgenic mice to generate four genotypes of mice: nonTg, 5xFAD, *Ppif*<sup>-/-</sup> and *Ppif*<sup>-/-</sup> 5xFAD mice. Genotypes of animals were confirmed using PCR and dot blot. All the studies were performed at age of 4 months (young) and 8–9 months (old) to mimic MCI and late-stage AD respectively. Both male and female animals were used in these studies.

#### 4.2. Human samples

Frozen brain samples were requested from UT Southwestern Medical Center ADC Neuropathology Core, supported by ADC grant (AG12300) under a protocol approved by The UT Southwestern Medical Center with informed consent from all subjects and study adhered to Declaration of Helsinki principles.

#### 4.3. Co-Immunoprecipitation of OSCP and CypD

Co-Immunoprecipitation was performed as previously described (Beck et al., 2016; Du et al., 2008). Human cortical tissues were lysed in buffer (50 mM Tris-HCl, 150 mM NaCl, 1 mM EDTA, 0.5% NP-40, 5% glycerol, and 1 × Protease inhibitor (Calbiochem), pH 7.4) by keeping on ice for 30 min, followed by 7 freeze and thaw cycles. Lysate was pelleted at 12,500 g at 4 °C and supernatant was used to immunoprecipitate OSCP using anti-OSCP (Santa Cruz Biotechnologies 0.5 μg IgG/100 μg protein) overnight at 4 °C. Pre-immuned IgG at the same concentration was used as the negative control. Prepared immuno-complex was incubated with pre-cleaned Protein agarose A/G (Pierce) for 2 h at room temperature. Beads were washed for 5 times to

remove non-specific binding of proteins. Western blot was performed and membrane was probed for anti-CypD (Calbiochem, 1:1000). The specific bands represent CypD co-immunoprecipitated with OSCP.

#### 4.4. Duolink® proximity ligation assay

Protein-protein interactions were detected using proximity ligation assay according to Duo-link in-situ detection (Sigma) protocol. The brain tissues were blocked for 30 min at 37 °C and subjected to primary antibodies: anti-OSCP (Santa Cruz Biotechnologies, 1: 200), anti-Aβ (CST, 1:1000) or anti-Cyclophilin D (Calbiochem, 1:200) for overnight at 4 °C. Following day, the slices were washed and treated with PLA probes for 1 h at 37 °C. The PLA probes were ligated at 37 °C for 30 min and the signal was amplified using polymerase for 2 h at 37 °C. DAPI was used as the nuclear stain. Tissues were mounted and imaged under Nikon confocal microscope followed by three-dimensional reconstruction and analysis using the NIS Advanced research software.

#### 4.5. Immunostaining for CypD and OSCP

Brain tissues from 4 and 9 months old nonTg and 5xFAD mice were used to perform co-staining of CypD and OSCP mitochondrial proteins. Citrate buffer was used to perform antigen retrieval followed by blocking in 5% goat serum and 0.3% triton-X for 1 h at RT. Primary antibodies: CypD (Calbiochem, 1:500) and OSCP (Santa Cruz, 1:400) were used in blocking buffer for overnight incubation. The next day, fluorescent-tagged secondary antibodies were used at the concentrations of 1:400 and washed. DAPI was used as the nuclear stain. Tissues were mounted and imaged under Nikon confocal microscope followed by three-dimensional reconstruction and analysis using the NIS Advanced research software.

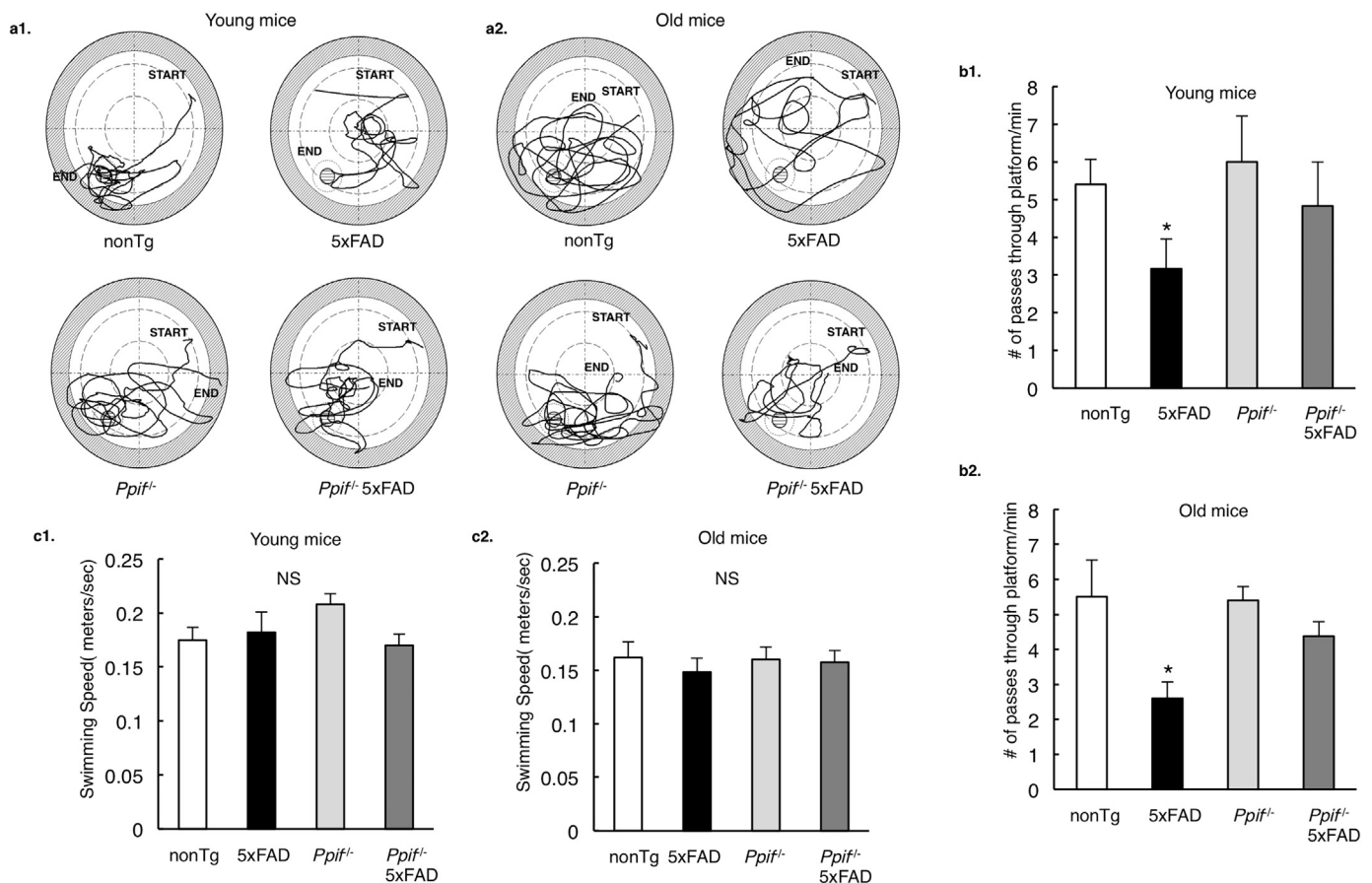


**Fig. 5.** CypD deficiency improves cognitive function in 5xFAD mice.

(a) Swimming traces for probe test after 11 days learning at Morris water maze for nonTg, *Ppif*<sup>-/-</sup> mice and their A $\beta$ -expressing counterparts at young and old ages. (b) 5xFAD mice demonstrated impaired learning ability to locate the hidden platform (in an age-dependent manner), which was protected in CypD deficient AD mice. \**P* < .05 vs other groups. (c) Mice in different groups did not display any difference in their swimming speeds. \**P* < .05 vs other groups. *n* = 6 for each group. Error bars represent s.e.m.

#### 4.6. GST-pulldown assay and binding curve

GST pulldown was performed according to manufacturer's protocol (Pierce). Briefly, the human OSCP cDNA (Gene Name: *ATP50*; NCBI Gene ID: 539) or human CypD cDNA (Gene Name: *Ppif*; NCBI Gene ID: 10105) was transformed into BL21 (DE3) pLysS *Escherichia coli* (Promega) using the pGEX-4t-1 plasmid (GE Healthcare). After transformation and selection a single colony was chosen for PCR to verify positive transformation. After overnight growth and induction by IPTG (Sigma-Aldrich), bacteria were pelleted and then were lysed by sonication in 1  $\times$  PBS containing 0.2 mM PMSF and 100  $\mu$ g ml<sup>-1</sup> lysozyme. After sonication bacterial debris was removed by centrifugation at 12,000g for 15 min at 4  $^{\circ}$ C. Supernatant was collected and incubated with glutathione agarose high-capacity, high-performance resin (Pierce) for 2 h. Glutathione beads were then washed and incubated overnight at 4  $^{\circ}$ C with purified hCypD protein or A $\beta$  peptide (ApexBio). After washing, protein was eluted from the beads and separated by SDS-PAGE. Coomassie blue staining was performed to visualize results. Binding curve was plotted using the arbitrary units using Graphpad Prism 6 software.

#### 4.7. Purification of GST-fusion hCypD protein

GST-hCypD protein was pulled down from *E. coli* as described above. Glutathione beads (Pierce) bound to the fusion protein were subjected to thrombin proteases (GE) to cleave the protein from GST. The cleaved hCypD protein were collected, then subjected to removal of

thrombin protease by using Hi-Trap Benzamidine FF (high sub) column (GE). The purified hCypD protein was concentrated into 1  $\times$  PBS using Amicon Ultra filtration units (Millipore) and protein concentration was determined using Bradford assay. Coomassie staining the protein on SDS-PAGE determined the purity of the protein.

#### 4.8. A $\beta$ staining

Mice brain tissues from both 4 and 9 months old 5xFAD and *Ppif*<sup>-/-</sup> 5xFAD mice were stained with A $\beta$  to determine the levels of A $\beta$ 42 deposition. Briefly, the brain tissues were blocked in 5% goat serum and 0.3% triton-X for 1 h at RT. Primary antibody A $\beta$  (CST, 1:1000) in blocking buffer was used for overnight incubation to allow staining. The next day, fluorescent-tagged secondary antibody was used at the concentration of 1:400 along with Nissl Blue stain (Sigma) and washed with 1  $\times$  PBS. Tissues were mounted and imaged under Nikon inverted microscope followed by analysis using the NIS Advanced research software.

#### 4.9. ELISA for amyloid $\beta$ levels

Synaptic amyloid  $\beta$  levels were measured using human Amyloid  $\beta$ (1–40) and Amyloid  $\beta$ (1–42) ELISA kit (Thermo Fisher Scientific) according to manufacturer's instructions.

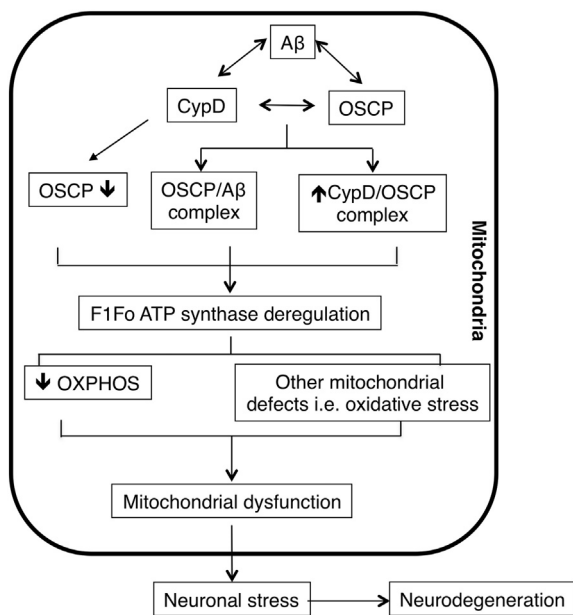


**Fig. 6.** Schematic summary.

In response to A $\beta$  deposition in AD brain mitochondria, CypD expression levels increase, which may promote OSCP reduction. Such changes potentiate elevated CypD/A $\beta$ , CypD/OSCP and OSCP/A $\beta$  interactions, leading to F1Fo ATP synthase dysfunction. The deregulation of this critical mitochondrial enzyme compromises mitochondrial OXPHOS efficacy and causes other mitochondrial defects including increased oxidative stress and calcium perturbations. Finally, the neuronal mitochondrial stress results in neuronal injury and eventually neurodegeneration.

#### 4.10. Synaptic mitochondria isolation

Mice brain synaptic mitochondria were isolated using density gradient centrifugation as previously described (Beck et al., 2016). Firstly, cortices from mice brain were homogenized in ice-cold mitochondria isolation buffer (225 mM mannitol, 75 mM sucrose, 2 mM K<sub>2</sub>PO<sub>4</sub>, 0.1% BSA, 5 mM Hepes, 1 mM EGTA (pH 7.2)) with a Dounce homogenizer (Wheaton). The homogenate were pelleted at 1300g for 5 min and the supernatant was layered on a 3 × 2-ml discontinuous gradient of 15, 23 and 40% (vol/vol) Percoll (GE) and centrifuged at 34,000 g for 8 min (flying time) on Beckman Coulter ultracentrifuge (Optima XPN-90 Ultracentrifuge). The band between 15 and 23% (containing synaptosomes) was collected. The fractions were then resuspended in isolation buffer containing 0.02% digitonin and incubated on ice for 5 min and then centrifuged at 16,500 g for 15 min. Pellets were collected and resuspended in isolation buffer. Percoll density gradient centrifugation was performed as described above for a second time. The interface between 23 and 40% (mitochondria released from synaptosomes) was collected and resuspended in isolation buffer to centrifuge at 16,500 g for 15 min. The resultant pellet was resuspended in isolation buffer followed by a centrifugation at 8000 g for 10 min. The final synaptic mitochondrial pellet was resuspended in isolation buffer and stored on ice during experiments. Protein concentration was determined using the Bio-Rad protein assay (Bio-Rad Laboratories).

#### 4.11. F1FO ATP synthase enzyme activity assay

F1FO ATP synthase enzymatic activity was measured spectrophotometrically using NADH-linked ATP regenerating system as previously described (Beck et al., 2016). 15  $\mu$ g of synaptic mitochondria was suspended in the assay buffer [100 mM Tris-HCl (pH 7.4), 2 mM MgCl<sub>2</sub>, 50 mM KCl, 0.2 mM EDTA, 0.23 mM NADH, and 1 mM Phosphoenolpyruvate]. The reaction was triggered by the addition of 0.4 M ATP-Mg and recorded at OD340nm on a spectrophotometer

(Ultraspect2100, Amersham Biosciences) for a total of 600 s at 10-second intervals and expressed in fold change.

#### 4.12. F1FO ATP synthase coupling assay

The coupling assay was performed as previously described (Beck et al., 2016). Synaptic mitochondria were treated with various concentrations of oligomycin A for 10 min at room temperature before conducting ATP synthase catalytic activity assay.

#### 4.13. Mitochondrial respiration assay

Freshly prepared synaptic mitochondria were used to perform this assay. Oxygen consumption was measured polarographically using temperature regulated Clark-type oxygen electrode (Oxytherm, Hansatech) as described previously (Du et al., 2008). In short, mitochondria were added to the magnetically stirred chamber and energized using 50  $\mu$ M of Glutamate-Malate (Sigma), followed by addition of substrate (ADP, Sigma, 300  $\mu$ M). State II respiration was measured as the oxygen consumption in the absence of the substrate, while addition of ADP induced state III respiration. On using up the substrate, a reduced rate of oxygen consumption was defined as the State IV respiration. Respiration Control ratio was measured as state III respiration over state IV respiration.

#### 4.14. Mitochondrial ATP synthesis measurements

ATP synthesis from freshly prepared synaptic mitochondria was measured using Luminescence ATP detection Assay Kit (Abcam) according to manufacturer's instructions. 15  $\mu$ g of isolated synaptic mitochondria were energized using 50  $\mu$ M of Glutamate/Malate, followed by addition of substrate (ADP, Sigma, 200  $\mu$ M). Luminescence was detected using a Microplate Reader (Synergy Mx., Biotek) with Gen5 software. Standard curve was prepared using ATP as substrate and luminescence readings were expressed in fold change.

#### 4.15. Immunoblotting

Immunoblotting was performed to quantify the expression levels of various proteins in isolated synaptic mitochondrial lysates. Proteins were separated in 12% Bis-Tris Gel (NuPAGE, Life Technologies) and then transferred to PVDF membrane (ImmunBlot Membrane, BioRad). Membranes were blocked with 5% non-fat dry milk (LabScientific Inc.) for 1 h at room temperature and probed with appropriate primary antibodies overnight at 4 °C; followed by the incubation with the appropriate secondary antibody for 1 h at room temperature. Proteins were detected using ECL (Clarity Substrate, BioRAD) and imaged using a Chemidoc system (BioRAD). The following antibodies were used in the experiments: anti-Cyclophilin D (Calbiochem, 1:5000), anti-Tom 40 (Santa Cruz, 1: 500), and for all the major F1FO ATP synthase subunits: anti-OSCP (Santa Cruz Biotechnologies, 1: 5000), anti- $\alpha$  subunit (Santa Cruz Biotechnologies, 1: 5000), anti- $\beta$  subunit (Santa Cruz Biotechnologies, 1: 5000), anti-a subunit (ProteinTech, 1: 5000), anti-b subunit (Santa Cruz Biotechnologies, 1: 500), anti- $\gamma$  subunit (Santa Cruz Biotechnologies, 1: 500), anti-c subunit (Abcam, 1:5000) and anti-Amyloid  $\beta$  (CST, 1:2000) The intensities of the immunoreactive bands were analyzed using ImageJ software from NIH.

#### 4.16. Whole brain mitochondria isolation

Brain mitochondria were prepared as previously described (Du et al., 2008). Cortices were dissected from mouse brain and homogenized in ice cold mitochondria isolation buffer (225 mM mannitol, 75 mM sucrose, 2 mM K<sub>2</sub>PO<sub>4</sub>, 0.1% BSA, 5 mM Hepes, 1 mM EGTA) with a dounce homogenizer (Wheaton). After a centrifugation at 1300 × g for 5 min to remove blood and cell debris, the supernatant was

layered on 15% Percoll (GE) and centrifuged at 12,500 ×g for 10 min. The pellet was collected and resuspended in isolation buffer with 0.02% Digitonin (Sigma-Aldrich) and then subjected to the second centrifugation at 8000 ×g for another 10 min. The pellet was then washed by additional centrifugation step in ice-cold isolation buffer without EGTA for experiments. Protein concentrations were measured using Bradford assay for protein detection (BioRad).

#### 4.17. Ubiquitination of OSCP

Immunoprecipitation was performed as previously described (Beck et al., 2016; Du et al., 2008). Freshly isolated mitochondria were lysed in buffer (50 mM Tris-HCl, 150 mM NaCl, 1 mM EDTA, 0.5% NP-40, 5% glycerol, and 1 × Protease inhibitor (Calbiochem), pH 7.4) by keeping on ice for 30 min, followed by 7 freeze and thaw cycles. Lysate was pelleted at 12,500g at 4 °C and supernatant was used to immunoprecipitate OSCP using anti-OSCP (Santa Cruz Biotechnologies 0.5 µg IgG/100 µg protein) overnight at 4 °C. Preimmuned IgG at the same concentration was used as the negative control. Prepared immuno-complex was incubated with pre-cleaned Protein agarose A/G (Pierce) for 2 h at room temperature. Beads were washed for 5 times to remove non-specific binding of proteins. Western blot was performed and membrane was probed for anti-Ub (Santa Cruz, 1:2000). The specific bands represent poly-ubiquitinated OSCP.

#### 4.18. Primary neuron culture

Primary neuron culture was performed using the established protocol. Briefly, brain tissues were dissected from day 0 pups and immersed in cold Hank's balanced salt solution (HBSS, Sigma-Aldrich), dissociated with 0.05% trypsin (Sigma-Aldrich) at 37 °C for 25–30 min followed by 10–15 times trituration. The cells were filtered through 40 µm mesh cell strainer (Fisher brand) and centrifuged for 5 min at 280 g. The pellet was gently resuspended in neuron culture medium (Neurobasal A with 2% B27 supplement and 0.5 mM L-glutamine, Gibco) and plated on poly-D-lysine (Sigma-Aldrich) coated culture plates (Corning) or chamber slides (Nunc) with an appropriate density. 10 µM 5-fluoro-2'-deoxyuridine (Sigma-Aldrich) was added to the neuron cultures to inhibit non-neuronal cell proliferation. Neurons were cultured to 12 days in vitro (DIV) for experiment.

#### 4.19. CypD overexpression in neurons

Human CypD cDNA (Gene Name: *Ppif*<sup>-/-</sup> NCBI Gene ID: 10105) were inserted in to lentivirus vector with human polyubiquitin promoter-C(Addgene). Lentiviruses were packaged and applied on primary neurons. The cells were treated with lentivirus for 5 days followed by their collection in 1 × LDS buffer followed by immunoblotting.

#### 4.20. Behavior studies

Morris water maze was performed to evaluate the mice spatial learning and reference memory according to previously described protocol (Beck et al., 2016). Briefly, mice were trained to find a submerged platform in an open swimming arena. Repeated trials ( $n = 4$ ) were performed each day for 11 days by starting the mice at random start locations (NW, N, NE, E, SE) while platform was fixed at a single location (SW). Each trial lasted 60 s with an additional 30 s learning time where mice were allowed to remain on the platform. After 11 days of learning, mice were subjected to a probe test in which the platform was removed. Mice were analyzed for number of times they passed previous learning time platform location (SW). HVS Image 2015 software (HVS Image) determined swimming speeds and analyzed the behavior data.

## Acknowledgement

This work was supported by research funding from NIH (R01AG053588, R01 AG059753), and Alzheimer's Association (AARG-16-442863).

## Conflict of interest

The authors have no conflict of interest to claim.

## Appendix A. Supplementary data

Supplementary data to this article can be found online at <https://doi.org/10.1016/j.nbd.2018.09.020>.

## References

- Baines, C.P., et al., 2005. Loss of cyclophilin D reveals a critical role for mitochondrial permeability transition in cell death. *Nature* 434, 658–662.
- Beck, S.J., et al., 2016. Deregulation of mitochondrial F1FO-ATP synthase via OSCP in Alzheimer's disease. *Nat. Commun.* 7, 11483.
- Beutner, G., et al., 2017. Cyclophilin D regulates the dynamic assembly of mitochondrial ATP synthase into synthasomes. *Sci. Rep.* 7, 14488.
- Carbajo, R.J., et al., 2007. How the N-terminal domain of the OSCP subunit of bovine F1FO-ATP synthase interacts with the N-terminal region of an alpha subunit. *J. Mol. Biol.* 368, 310–318.
- Chinopoulos, C., et al., 2011. Modulation of F0F1-ATP synthase activity by cyclophilin D regulates matrix adenine nucleotide levels. *FEBS J.* 278, 1112–1125.
- Cummings, J.L., 2004. Alzheimer's disease. *N. Engl. J. Med.* 351, 56–67.
- Dahout-Gonzalez, C., et al., 2006. Molecular, functional, and pathological aspects of the mitochondrial ADP/ATP carrier. *Physiology (Bethesda)* 21, 242–249.
- Du, H., Yan, S.S., 2010. Mitochondrial permeability transition pore in Alzheimer's disease: cyclophilin D and amyloid beta. *Biochim. Biophys. Acta* 1802, 198–204.
- Du, H., et al., 2008. Cyclophilin D deficiency attenuates mitochondrial and neuronal perturbation and ameliorates learning and memory in Alzheimer's disease. *Nat. Med.* 14, 1097–1105.
- Du, H., et al., 2010. Early deficits in synaptic mitochondria in an Alzheimer's disease mouse model. *Proc. Natl. Acad. Sci. U. S. A.* 107, 18670–18675.
- Du, H., et al., 2011. Cyclophilin D deficiency improves mitochondrial function and learning/memory in aging Alzheimer disease mouse model. *Neurobiol. Aging* 32, 398–406.
- Du, H., et al., 2012. Synaptic mitochondrial pathology in Alzheimer's disease. *Antioxid. Redox Signal.* 16, 1467–1475.
- Gauba, E., et al., 2017. Cyclophilin D promotes brain mitochondrial F1FO ATP synthase dysfunction in aging mice. *J. Alzheimers Dis.* 55, 1351–1362.
- Giorgio, V., et al., 2009. Cyclophilin D modulates mitochondrial F0F1-ATP synthase by interacting with the lateral stalk of the complex. *J. Biol. Chem.* 284, 33982–33988.
- Giorgio, V., et al., 2010. Cyclophilin D in mitochondrial pathophysiology. *Biochim. Biophys. Acta* 1797, 1113–1118.
- He, J., et al., 2018. Assembly of the membrane domain of ATP synthase in human mitochondria. *Proc. Natl. Acad. Sci. U. S. A.* 115, 2988–2993.
- Heo, J.M., Rutter, J., 2011. Ubiquitin-dependent mitochondrial protein degradation. *Int. J. Biochem. Cell Biol.* 43, 1422–1426.
- Koos, B., et al., 2014. Analysis of protein interactions in situ by proximity ligation assays. *Curr. Top. Microbiol. Immunol.* 377, 111–126.
- Lebedev, I., et al., 2016. A novel in vitro CypD-mediated p53 aggregation assay suggests a model for mitochondrial permeability transition by chaperone systems. *J. Mol. Biol.* 428, 4154–4167.
- Lehmann, G., et al., 2016. Ubiquitination of specific mitochondrial matrix proteins. *Biochem. Biophys. Res. Commun.* 475, 13–18.
- Lutz, M.I., et al., 2017. Novel approach for accurate tissue-based protein colocalization and proximity microscopy. *Sci. Rep.* 7, 2668.
- Manczak, M., et al., 2004. Differential expression of oxidative phosphorylation genes in patients with Alzheimer's disease: implications for early mitochondrial dysfunction and oxidative damage. *NeuroMolecular Med.* 5, 147–162.
- Margineantu, D.H., et al., 2007. Hsp90 inhibition decreases mitochondrial protein turnover. *PLoS One* 2, e1066.
- Mastroeni, D., et al., 2017. Nuclear but not mitochondrial-encoded oxidative phosphorylation genes are altered in aging, mild cognitive impairment, and Alzheimer's disease. *Alzheimers Dement.* 13, 510–519.
- Nguyen, T.T., et al., 2013. Cyclophilin D modulates mitochondrial acetylome. *Circ. Res.* 113, 1308–1319.
- Onyango, I.G., et al., 2016. Mitochondrial dysfunction in Alzheimer's disease and the rationale for bioenergetics based therapies. *Aging Dis.* 7, 201–214.
- Reddy, P.H., 2006. Mitochondrial oxidative damage in aging and Alzheimer's disease: implications for mitochondrially targeted antioxidant therapeutics. *J. Biomed. Biotechnol.* 2006, 31372.
- Reddy, P.H., Beal, M.F., 2008. Amyloid beta, mitochondrial dysfunction and synaptic damage: implications for cognitive decline in aging and Alzheimer's disease. *Trends Mol. Med.* 14, 45–53.

- Reddy, P.H., et al., 2010. Amyloid-beta and mitochondria in aging and Alzheimer's disease: implications for synaptic damage and cognitive decline. *J. Alzheimers Dis.* 20 (Suppl. 2), S499–S512.
- Rubinstein, J.L., et al., 2003. Structure of the mitochondrial ATP synthase by electron cryomicroscopy. *EMBO J.* 22, 6182–6192.
- Swerdlow, R.H., et al., 2014. The Alzheimer's disease mitochondrial cascade hypothesis: progress and perspectives. *Biochim. Biophys. Acta* 1842, 1219–1231.
- Wang, X., et al., 2014. Oxidative stress and mitochondrial dysfunction in Alzheimer's disease. *Biochim. Biophys. Acta* 1842, 1240–1247.
- Wang, L., et al., 2016. Synaptosomal Mitochondrial Dysfunction in 5xFAD Mouse Model of Alzheimer's Disease. *PLoS One* 11, e0150441.
- Wedemeyer, W.J., et al., 2002. Proline cis-trans isomerization and protein folding. *Biochemistry* 41, 14637–14644.
- Woodfield, K., et al., 1998. Direct demonstration of a specific interaction between cyclophilin-D and the adenine nucleotide translocase confirms their role in the mitochondrial permeability transition. *Biochem. J.* 336, 287–290 Pt 2.
- Wu, Y., Matthews, C.R., 2002. A cis-prolyl peptide bond isomerization dominates the folding of the alpha subunit of Trp synthase, a TIM barrel protein. *J. Mol. Biol.* 322, 7–13.
- Yao, J., et al., 2009. Mitochondrial bioenergetic deficit precedes Alzheimer's pathology in female mouse model of Alzheimer's disease. *Proc. Natl. Acad. Sci. U. S. A.* 106, 14670–14675.
- Zhu, X., et al., 2013. Abnormal mitochondrial dynamics in the pathogenesis of Alzheimer's disease. *J. Alzheimers Dis.* 33 (Suppl. 1), S253–S262.